



**Please cite the Published Version**

Goyal, M, Reeves, ND , Rajbhandari, S, Ahmad, N, Wang, C and Yap, MH  (2020) Recognition of ischaemia and infection in diabetic foot ulcers: Dataset and techniques. *Computers in Biology and Medicine*, 117. ISSN 0010-4825

**DOI:** <https://doi.org/10.1016/j.compbiomed.2020.103616>

**Publisher:** Elsevier

**Version:** Accepted Version

**Downloaded from:** <https://e-space.mmu.ac.uk/625080/>

**Usage rights:**  [Creative Commons: Attribution-Noncommercial-No Derivative Works 4.0](https://creativecommons.org/licenses/by-nc-nd/4.0/)

**Additional Information:** This is an Open Access article published in *Computers in Biology and Medicine*, published by Elsevier, copyright The Author(s).

**Enquiries:**

If you have questions about this document, contact [openresearch@mmu.ac.uk](mailto:openresearch@mmu.ac.uk). Please include the URL of the record in e-space. If you believe that your, or a third party's rights have been compromised through this document please see our Take Down policy (available from <https://www.mmu.ac.uk/library/using-the-library/policies-and-guidelines>)

# Recognition of Ischaemia and Infection in Diabetic Foot Ulcers: Dataset and Techniques

Manu Goyal<sup>a</sup>, Neil D. Reeves<sup>b</sup>, Satyan Rajbhandari<sup>c</sup>, Naseer Ahmad<sup>d</sup>,  
Chuan Wang<sup>e</sup>, Moi Hoon Yap<sup>a,\*</sup>

<sup>a</sup>*Centre for Advanced Computational Sciences, Manchester Metropolitan University, M1 5GD, Manchester, UK*

<sup>b</sup>*Research Centre for Musculoskeletal Science & Sports Medicine, Manchester Metropolitan University, M1 5GD, Manchester, UK.*

<sup>c</sup>*Lancashire Teaching Hospital, PR2 9HT, Preston, UK.*

<sup>d</sup>*University of Manchester and Manchester Royal Infirmary, M13 9WL, Manchester, UK.*

<sup>e</sup>*Department of Endocrinology, Sun Yat-sen Memorial Hospital, Sun Yat-sen University, Guangzhou 510120, P.R. China.*

---

## Abstract

Recognition and analysis of Diabetic Foot Ulcers (DFU) using computerized methods is an emerging research area with the evolution of image-based machine learning algorithms. Existing research using visual computerized methods mainly focuses on recognition, detection, and segmentation of the visual appearance of the DFU as well as tissue classification. According to DFU medical classification systems, the presence of infection (bacteria in the wound) and ischaemia (inadequate blood supply) has important clinical implications for DFU assessment, which are used to predict the risk of amputation. In this work, we propose a new dataset and computer vision techniques to identify the presence of infection and ischaemia in DFU. This is the first time a DFU dataset with ground truth labels of ischaemia and infection cases is introduced for research purposes. For the handcrafted machine learning approach, we propose a new feature descriptor, namely the Superpixel Color Descriptor. Then we use the Ensemble Convolutional Neural Network (CNN) model for more effective recognition of ischaemia and infection. We propose to use a natural data-augmentation method, which

---

\*Corresponding author: Tel.: +44 161 247 1503;  
*Email address: M.Yap@mmu.ac.uk (Moi Hoon Yap )*

identifies the region of interest on foot images and focuses on finding the salient features existing in this area. Finally, we evaluate the performance of our proposed techniques on binary classification, i.e. ischaemia versus non-ischaemia and infection versus non-infection. Overall, our method performed better in the classification of ischaemia than infection. We found that our proposed Ensemble CNN deep learning algorithms performed better for both classification tasks as compared to handcrafted machine learning algorithms, with 90% accuracy in ischaemia classification and 73% in infection classification.

*Keywords:*

Diabetic foot ulcers, deep learning, ischaemia, infection, machine learning.

---

## 1 Introduction

Diabetic Foot Ulcers (DFUs) are a major complication of diabetes which can lead to amputation of the foot or limb. Treatment of Diabetic foot ulcers is a global major health care problem resulting in high care costs and mortality rate. Recognition of infection and ischaemia is very important to determine factors that predict the healing progress of DFU and the risk of amputation. Ischaemia, the lack of blood circulation, develops due to chronic complications of diabetes. This can result in gangrene of the diabetic foot ulcer, which may require amputation of the part of the foot or leg if not recognised and treated early. Detailed knowledge of the vascular anatomy of the leg, and particularly ischaemia enables medical experts make better decisions in estimating the possibility of DFU healing, given the existing blood supply [1]. In previous studies, it is estimated that patients with critical ischaemia have a three-year limb loss rate of about 40% [2]. Patients with an active DFU and particularly those with ischaemia or gangrene should be checked for the presence of infection. Approximately, 56% of DFU become infected and 20% of DFU infections lead to amputation of a foot or limb [3, 4, 5]. In one recent study, 785 million patients with diabetes in the US between 2007 and 2013 suggested that DFU and associated infections constitute a powerful risk factor for emergency department visits and hospital admission [6].

There are a number of DFU classification systems such as Wagner, University of Texas, and SINBAD Classification systems, which include information on the site of DFU, area, depth, presence of neuropathy, presence of

25 ischaemia, and infection [7, 8, 9]. SINBAD stands for S (Site), I (Ischaemia),  
26 N (Neuropathy), B (Bacterial infection), A (Area), D (Depth). This paper  
27 focuses on ischaemia and infection, which are defined as follow:

- 28 1. Ischaemia: Inadequate blood supply that could affect DFU healing.  
29 Ischaemia is diagnosed by palpating foot pulses and measuring blood  
30 pressure in the foot and toes. The visual appearance of ischaemia might  
31 be indicated by the presence of poor reperfusion to the foot, or black  
32 gangrenous toes (tissues death to part of the foot). From a computer  
33 vision perspective, these might be important hints of the presence of  
34 ischaemia in the DFU.
- 35 2. Bacterial Infection: Infection is defined as bacterial soft tissue or bone  
36 infection in the DFU, which is based on the presence of at least two  
37 classic findings of inflammation or purulence. It is very hard to de-  
38 termine the presence of diabetic foot infections from DFU images, but  
39 increased redness in and around ulcer and coloured purulent could pro-  
40 vide indications. In the medical system, blood testing is performed as  
41 the gold standard diagnostic test. Also, in the present dataset, the  
42 images were captured after the debridement of necrotic and devital-  
43 ized tissues which removes an important indication of the presence of  
44 infection in DFU.

45 In related work, Netten et al. [10] find that clinicians achieved low validity  
46 and reliability for remote assessment of DFU in foot images. Hence, it is clear  
47 that analysing these conditions from images is a difficult task for clinicians.  
48 In various image recognition applications, such as medical imaging and natu-  
49 ral language processing tasks, machine learning algorithms performed better  
50 than skilled humans including clinicians [11, 12, 13].

51 The previous state-of-the-art image-based computer-aided diagnosis of  
52 DFU is composed of multiple stages, including image pre-processing, image  
53 segmentation, feature extraction, and classification. Veredas et al. [14] pro-  
54 posed the use of color and texture features from the segmented area and  
55 multi-layer neural network to perform the tissue classification to distinguish  
56 between healing-tissue and skin for healing prediction. Wannous et al. [15]  
57 performed tissue classification from color and texture region descriptors on  
58 a 3-D model for the wound. Wang et al. [16] used a cascaded two-stage  
59 classifier to determine the DFU boundaries for area determination of DFU.  
60 Major progress in the field of image-based machine learning, especially deep

61 learning algorithms, allows the extensive use of medical imaging data with  
62 end-to-end models to provide better diagnosis, treatment, and prediction of  
63 diseases [17, 18]. Deep learning models for DFU, predominantly led by works  
64 from our laboratory have achieved high accuracy in the recognition of DFUs  
65 with machine learning algorithms [19, 20, 21, 22].

66 The major issues and challenges involved with the assessment of DFU  
67 using machine learning methods from foot images are as follows: 1) a major  
68 time-burden involved in data collection and expert labelling of the DFU  
69 images; 2) high inter-class similarity and intra-class variations are dependent  
70 upon the different classification of DFU; 3) non-standardization of the DFU  
71 dataset, such as distance of the camera from the foot, orientation of the image  
72 and lighting conditions; 4) lack of meta-data, such as patient ethnicity, age,  
73 sex and foot size.

74 Accurate diagnosis of ischaemia and infection requires establishing a good  
75 clinical history, physical examination, blood tests, bacteriological study and  
76 Doppler study of leg blood vessels. These tests and resources are not always  
77 available to clinicians across the world and hence the need for a solution to  
78 inform diagnosis, such as the one we proposed in this paper. Experts working  
79 in the field of diabetic foot ulceration have good experience of predicting the  
80 presence of underlying ischaemia or infection simply by looking at the ulcer.  
81 We aim to replicate that in machine learning. To increase the reliability of  
82 the annotation, two experts predict the presence of ischaemia and infection  
83 from DFU images. Due to high risks of infection and ischaemia in DFU  
84 leading to patient’s hospital admission, and amputation [23], recognition of  
85 infection and ischaemia in DFU with cost-effective machine learning methods  
86 is a very important step towards the development of complete computerized  
87 DFU assessment system for remote monitoring in the future.

## 88 **2. DFU Dataset and Expert Labelling**

89 For binary classification of ischaemia and infection in DFU, we introduce  
90 a dataset of 1459 images of patient’s foot with DFU over the previous five  
91 years at the Lancashire Teaching Hospitals, obtaining ethical approval from  
92 all relevant bodies and patients written informed consent. Approval was ob-  
93 tained from the NHS Research Ethics Committee to use these images for this  
94 research. These DFU images were captured with different cameras (Kodak  
95 DX4530, Nikon D3300, and Nikon COOLPIX P100). The current dataset



Figure 1: Examples of foot images with DFU used for binary expert annotations for infection and ischaemia.

96 we received with the ethical approval from NHS did not contain any records  
 97 or meta-data about these conditions or any medical classification.

98 Since there is no clinical meta-data regarding this DFU dataset, the ex-  
 99 periment is performed on the images with handcrafted traditional machine  
 100 learning and deep learning. This is the first time, recognition of ischaemia  
 101 and infection in DFU is performed based on images, hence, there is no pub-  
 102 licly available dataset. Here, we introduce the first DFU dataset with ground  
 103 truth labels of ischaemia and infection cases. Expert labelling of each DFU

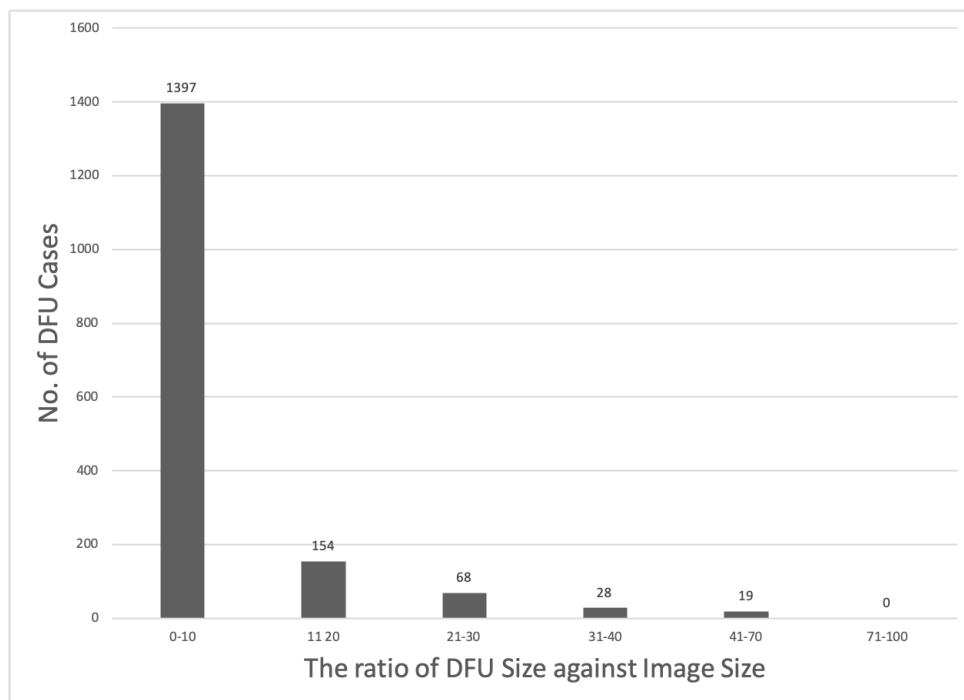


Figure 2: The number of DFU cases according to the area of DFU in full foot image of the DFU dataset.

104 according to the different conditions present in DFU according to the pop-  
105 ular medical classification system on this DFU dataset is particularly im-  
106 portant for this task. The ground truth was produced by two healthcare  
107 professionals (consultant physicians with specialisation in the diabetic foot)  
108 on the visual inspection of DFU images. Where there was disagreement for  
109 the ground truth, the final decision was made by the more senior physician.  
110 These ground truths are used for the binary classification of infection and  
111 ischaemia of DFU. A few examples of foot images with DFU used for bi-  
112 nary expert annotation are shown in Fig. 1. The complete number of cases  
113 of expert annotation of each condition is detailed in Table 1. The dataset,  
114 alongside its ground truth labels, will be made available upon acceptance of  
115 this article.

### 116 3. Methodology

117 This section describes our proposed techniques for the recognition of is-  
118 chaemia and infection of the DFU diagnosis system. The preparation of  
119 a balanced dataset, handcrafted features, and machine learning methods  
120 (handcrafted machine learning and deep learning approaches) used for bi-  
121 nary classification of ischaemia and infection are detailed in this section.

#### 122 3.1. Natural Data-Augmentation Technique based on Deep Learning Algo- 123 rithm

124 This section describes our proposed data augmentation method, called  
125 Natural Data-augmentation, which is based on deep DFU localization algo-  
126 rithm (Faster R-CNN).

127 In the DFU dataset, the images (size )varies between  $1600 \times 1200$  and  
128  $3648 \times 2736$ ) depending on the cameras used to capture the data. In deep  
129 learning, data augmentation is envisioned as an important tool to improve  
130 the performance of algorithms. As shown in Fig. 2, approximately 92% of  
131 DFU cases have area between 0% to 20% on foot images. In common data-  
132 augmentation, the number of techniques used such as flip, rotation, random  
133 scale, random crop, translation, and Gaussian noise to perform augment in  
134 the dataset. Since DFU occupies a very small percentage of the total area  
135 of foot images, there is a risk of missing the region of interests by using im-  
136 portant augmentation technique such as random scale, crop, and translation.  
137 Hence, Natural Data-augmentation is more suitable for the DFU evaluation  
138 rather than common data-augmentation. This augmentation technique helps



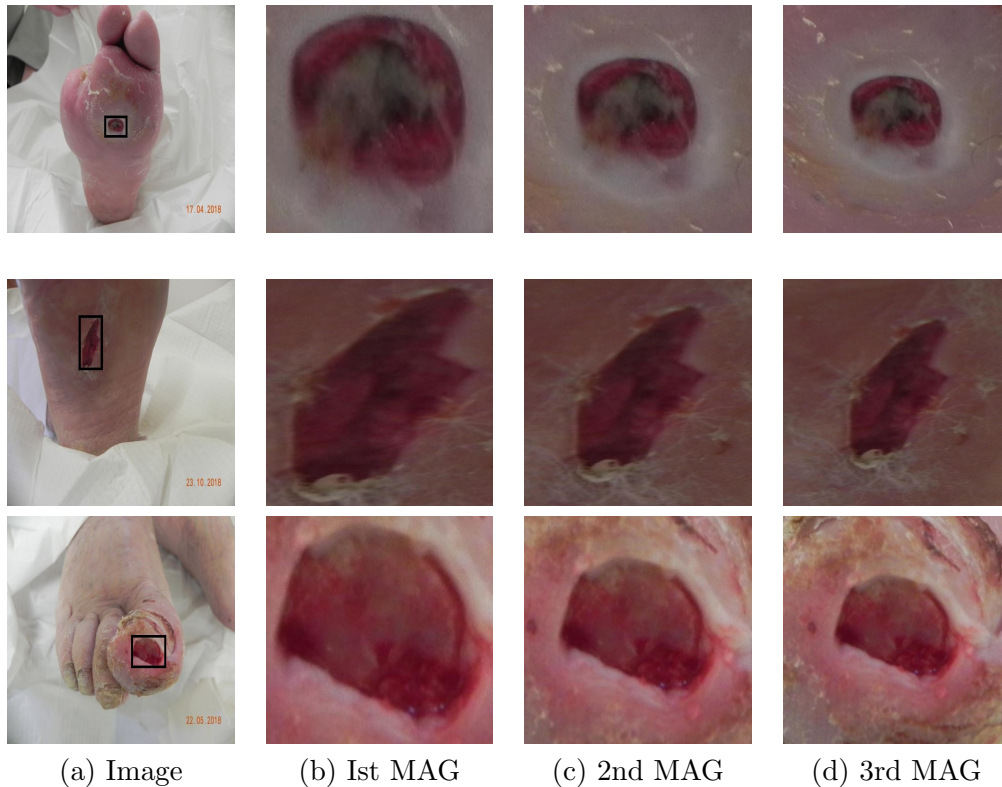


Figure 3: Natural Data-augmentation produced from the original image with different magnifications (three magnifications in this experiment). MAG refers to magnification

139 in assisting the machine algorithms to pinpoint ROI of DFU on foot images  
 140 and focus on finding the strong features that exists in this area. We used  
 141 the deep learning-based localization method, Faster-RCNN with Inception-  
 142 ResNetV2, to get ROI of the DFU on foot images [24, 25]. Depending upon  
 143 the size of DFU and image, the natural data-augmentation on the DFU  
 144 dataset with different magnification is demonstrated in Fig. 3. Flexible pa-  
 145 rameters can be used to choose the number of magnification factors (3 in  
 146 this classification), as well as magnification distance, which can be adjusted  
 147 from a single DFU image by natural augmentation. After magnification, fur-  
 148 ther, data-augmentation is achieved with the help of angles, mirror, gaussian  
 149 noise, contrast, sharpen, translation, shearing using our proposed methods  
 150 as shown in Fig. 4.

151 As shown in Table 1, the number of DFU patches generated by crop-  
 152 ping multiple DFU on foot images and augmented patches are generated

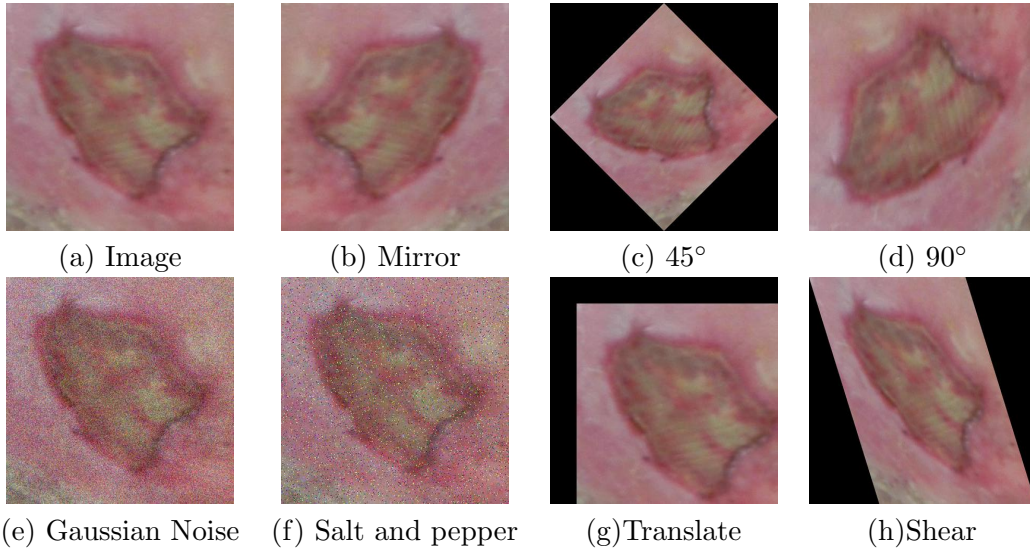


Figure 4: After magnification, different types of data-augmentation is achieved by the proposed Natural Data-augmentation

153 by natural data-augmentation (Fig. 3) and different data augmentations  
 154 (Fig. 4). The total number of cases for ischaemia and non-ischaemia in this  
 155 DFU dataset is imbalanced (1249 cases vs 210 cases) whereas infection (628  
 156 cases) and non-infection (831 cases) are fairly balanced as shown in Table 1.  
 157 We performed binary classification of ischaemia and infection with machine  
 158 learning algorithms because for multi-class classification, this DFU dataset  
 159 is imbalanced especially for cases (Ischaemia and No Infection) as shown in  
 160 5.

### 161 3.2. Handcrafted Superpixel Color Descriptors

162 We investigated the use of human design features with traditional machine  
 163 learning on the binary classification of infection and ischaemia. Our first  
 164 attempt was experimenting with texture descriptors (Local Binary Patterns  
 165 and Histogram of Gradient) and color descriptors as used in related works  
 166 [19, 21]. However, we achieved very poor results for these binary classification  
 167 problems. Hence, we propose a novel Superpixel Color Descriptors (SPCD)  
 168 to extract the colors region of interest from DFU images that could be the  
 169 important visual cues for the identification of ischaemia and infection in DFU.  
 170 In the first step, we used a SLIC superpixels technique to produce superpixel  
 171 over-segmentation of DFU patches based on pixel color and intensity values

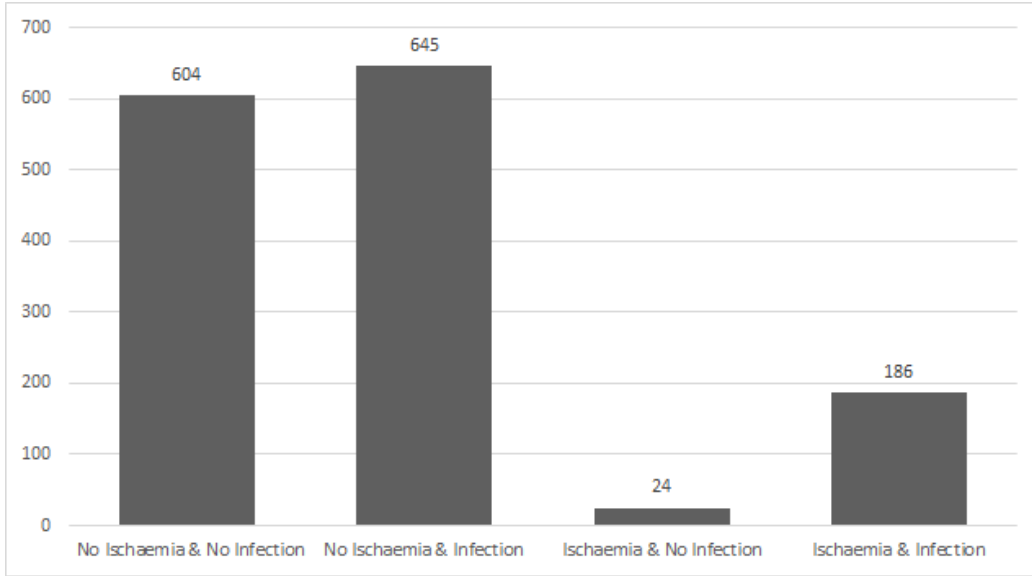


Figure 5: Distribution of ischaemia and infection cases as multi-class classification problem.

Table 1: The number of Infection and ischaemia cases, number of DFU patches and augmented patches using Natural Data-augmentation in DFU Dataset

Category	Definition	Cases	DFU patches	Augmented patches
Ischaemia	Absent	1249	1431	4935
	Present	210	235	4935
Total images		1459	1666	9870
Bacterial infection	None	628	684	2946
	Present	831	982	2946
Total images		1459	1666	5892

172 [26]. SLIC superpixels technique performs a localized  $k$ -means optimization  
 173 in the 5-D CIELAB color and image space to cluster pixels as described by  
 174 equations 1 - 4:

$$S = \sqrt{\frac{N}{k}} \quad (1)$$

$$D_s = d_{lab} + \frac{m}{S} d_{xy} \quad (2)$$

$$d_{lab} = \sqrt{(l_k - l_i)^2 + (a_k - a_i)^2 + (b_k - b_i)^2} \quad (3)$$

$$d_{xy} = \sqrt{(x_k - x_i)^2 + (y_k - y_i)^2} \quad (4)$$

175 where in eq. 1,  $S$  is the approximate size of a superpixel,  $N$  is the number  
 176 of pixels and  $k$  is the number of superpixels; in eq. 2,  $D_s$  is the sum of the lab  
 177 distance ( $d_{lab}$ ) and the xy plane distance ( $d_{xy}$ ); in eq. 3,  $l$ ,  $a$  and  $b$  represent  
 178 the lab colorspace; and in eq. 4,  $x$  and  $y$  represent the pixel positions.

179 In the second step, the mean RGB color value of each superpixel is com-  
 180 puted and applied to each superpixel ( $S$ ) denoted by:

$$S_i = \text{mean}(P(R, G, B)), i = 1, \dots, k \quad (5)$$

181 where in eq. 5,  $P(R, G, B)$  is the pixel values of R,G,B channel in each  $i$ th  
 182 position of  $S$  and  $k$  is total number of superpixels in the image.

183 Finally, with a different number of superpixels and threshold values from  
 184 each color channel, we extracted regions of two particular colors of inter-  
 185 est that are red and black from the DFU patches. For these classification  
 186 tasks, we used the number of superpixels ( $k=200$ ) and threshold values (T1:  
 187 0.40,0.45,0.50,.055,0.60; T2: 0.15,0.20,0.25,0.30,0.35) to extract the color fea-  
 188 tures from DFU patches of  $256 \times 256$ . The threshold values are used to restrict  
 189 the intensities of red and black pixels to be utilized as handcrafted features.  
 190 Hence, we utilised a feature vector of 10 with SPCD algorithm along with  
 191 texture descriptors (LBP, HOG) and color features (RGB, CIELAB) to train  
 192 traditional machine learning approaches. The pseudocode for the SPCD al-  
 193 gorithm is explained in Algorithm 1. The example of extracting color features  
 194 using our novel SPCD algorithm is shown in Fig. 6.

195 For these classification problems, we experimented with a number of clas-  
 196 sifiers with standard hyper-parameters on these color features. BayesNet,

---

**Algorithm 1** Pseudocode for the Superpixel Color Descriptors Extraction

---

- 1: Over-segmentation of DFU patch with SLIC superpixel is performed;
  - 2: Mean RGB value of each superpixel is calculated and applied;
  - 3: Initialize variable S\_Red & S\_Black to 0
  - 4: **procedure** REDANDBLACKREGION
  - 5:     **for** each Superpixel( $S_i$ ) **do**
  - 6:         **if**  $S_i(R) > T_1 * (S_i(R) + S_i(G) + S_i(B))$  **then return** S\_Red=  
S\_Red + 1
  - 7:         **if**  $S_i(R) < T_2 \ \& \ S_i(G) < T_2 \ \& \ S_i(B) < T_2$  **then return**  
S\_Black= S\_Black + 1
  - 8:          $RedColorFeature = S\_Red \div n$
  - 9:          $BlackColorFeature = S\_Black \div n$
- 

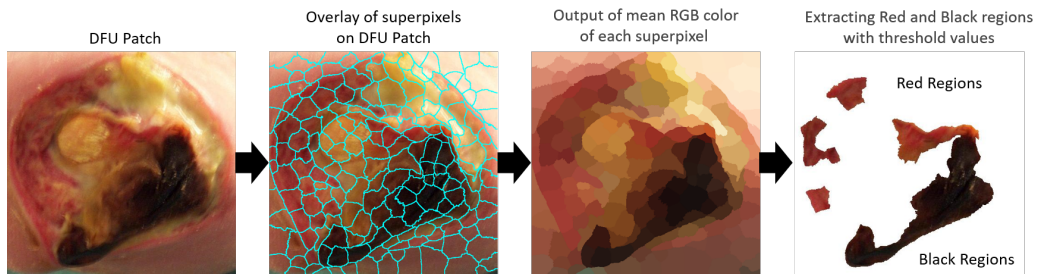


Figure 6: Example of extracting red and black regions from DFU patch with proposed Superpixel Color Descriptor algorithm which was then used to inform identification of ischaemia and infection. The k value of 200 for superpixel algorithm effectively oversegmented the DFU patches.

197 Random Forest, and Multilayer Perceptron were selected and achieved the  
198 highest accuracy among other machine learning classifiers.

### 199 *3.3. Deep Learning Approaches*

200 For comparison with the traditional features, deep learning algorithms  
201 are used to perform binary classification to classify (1) infection and non-  
202 infection; and (2) ischaemia and non-ischaemia classes in DFU patches. For  
203 this work, we fine-tune (transfer learning from pre-trained models) the CNN  
204 models, i.e. Inception-V3, ResNet50, and InceptionResNetV2 [27, 28, 29].  
205 To train the CNN networks, we froze the weights of the first few layers of  
206 the pre-trained networks for common features, such as edges and curves.  
207 Subsequently, layers of networks are unfrozen to focus on learning dataset-  
208 specific features.

209 Additionally, we utilized the Ensemble CNN method, which is a very  
210 effective CNN approach to obtain very good accuracy on difficult datasets.  
211 The Ensemble CNN model combines the bottleneck features from multiple  
212 CNN models (Inception-V3, ResNet50, and InceptionResNetV2), and use  
213 SVM classifier to produce predictions, as shown in Fig. 7.

## 214 **4. Results and Discussion**

215 Both infection and ischaemia datasets were split into 70% training, 10%  
216 validation and 20% testing sets and we adopted the 5-fold cross-validation  
217 technique. We utilized the natural data-augmentation technique for training  
218 and validation sets in both traditional machine learning and deep learning  
219 approaches. Hence, in this ischaemia dataset, we used approximately 11,564  
220 patches, 1,652 patches, and 3,304 patches in training, validation, and test-  
221 ing sets respectively whereas, in the infection dataset, we used 7,136 patches  
222 (training), 1,019 patches (validation), and 2,038 patches (testing) from the  
223 2611 original foot images. As mentioned previously, we used both hand-  
224 crafted traditional machine learning (henceforth TML) models and CNN  
225 models to perform the classification task and utilized  $256 \times 256$  RGB images  
226 as input for TML and InceptionV3, AlexNet, and ResNet50. For Inception-  
227 ResNetV2, we resized the dataset to  $299 \times 299$ . For this experiment, Tensor-  
228 Flow is used for deep learning and Matlab is used for traditional machine  
229 learning approaches.

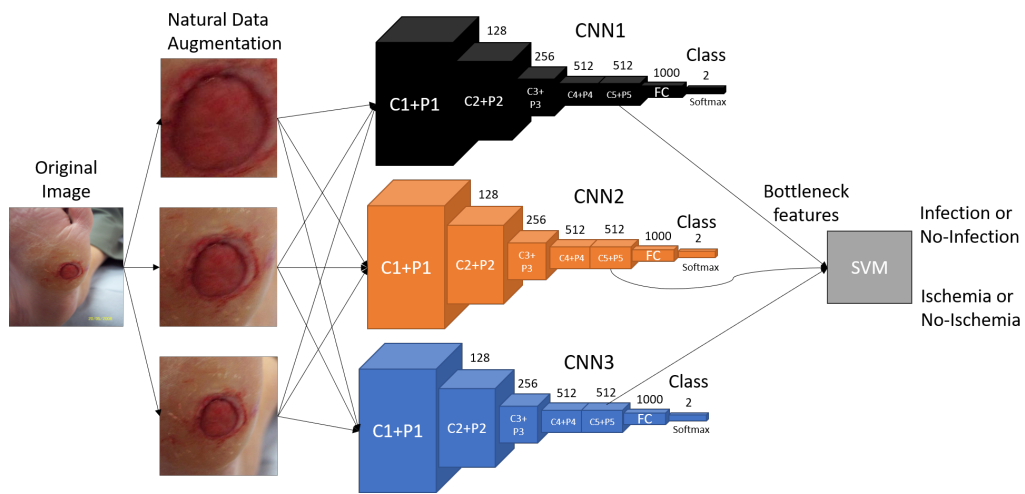


Figure 7: Extracting bottleneck features from CNNs and fed into SVM classifier to perform binary classification of ischaemia and infection, where C1-C5 are convolutional layers, P1-P5 are pooling layers and FC is fully connected layer. **Note: The CNNs in this figure are just representations of general CNNs architecture and do not represent the original CNN architectures of Inception-V3, ResNet50, and InceptionRes-NetV2.**

Table 2: The performance measures of binary classification of ischaemia by our proposed handcrafted traditional machine learning and CNN approaches.

	<i>Accuracy</i>	<i>Sensitivity</i>	<i>Precision</i>	<i>Specificity</i>	<i>F-Measure</i>	<i>MCC Score</i>	<i>AUC Score</i>
BayesNet	0.785±0.022	0.774±0.034	0.809±0.034	0.800±0.027	0.790±0.020	0.572±0.044	0.783
Random Forest	0.780±0.041	0.739±0.049	0.872±0.029	0.842±0.034	0.799±0.033	0.571±0.078	0.780
Multilayer Perceptron	0.804±0.022	0.817±0.040	0.787±0.046	0.795±0.031	0.800±0.023	0.610±0.045	0.804
InceptionV3 (CNN)	0.841±0.017	0.784±0.045	0.886±0.018	0.898±0.022	0.831±0.021	0.688±0.031	0.840
ResNet50 (CNN)	0.862±0.018	0.797±0.043	0.917±0.015	0.927±0.017	0.852±0.022	0.732±0.032	0.865
InceptionResNetV2 (CNN)	0.853±0.021	0.789±0.054	0.906±0.017	0.917±0.019	0.842±0.027	0.714±0.039	0.851
Ensemble (CNN)	<b>0.903±0.012</b>	<b>0.886±0.035</b>	<b>0.918±0.019</b>	<b>0.921±0.021</b>	<b>0.902±0.014</b>	<b>0.807±0.022</b>	<b>0.904</b>

Table 3: The performance measures of binary classification of Infection by our proposed handcrafted traditional machine learning and CNN approaches.

	<i>Accuracy</i>	<i>Sensitivity</i>	<i>Precision</i>	<i>Specificity</i>	<i>F-Measure</i>	<i>MCC Score</i>	<i>AUC Score</i>
BayesNet	0.639±0.036	0.619±0.018	0.653±0.039	0.660±0.015	0.622±0.079	0.290±0.070	0.643
Random Forest	0.605±0.025	0.608±0.025	0.607±0.037	0.601±0.069	0.606±0.012	0.211±0.051	0.601
Multilayer Perceptron	0.621±0.026	0.680±0.023	0.622±0.057	0.570±0.023	0.627±0.074	0.281±0.055	0.619
InceptionV3 (CNN)	0.662±0.014	0.693±0.038	0.653±0.015	0.631±0.034	0.672±0.019	0.325±0.029	0.662
ResNet50 (CNN)	0.673±0.013	0.692±0.051	0.668±0.023	0.654±0.051	0.679±0.019	0.348±0.028	0.673
InceptionResNetV2 (CNN)	0.676±0.015	0.688±0.052	0.672±0.015	0.664±0.039	0.680±0.024	0.352±0.031	0.678
Ensemble (CNN)	<b>0.727±0.025</b>	<b>0.709±0.044</b>	<b>0.735±0.036</b>	<b>0.744±0.050</b>	<b>0.722±0.028</b>	<b>0.454±0.052</b>	<b>0.731</b>

230 In Table 2 and 3, we report *Accuracy*, *Sensitivity*, *Precision*, *Specificity*, *F-*  
231 *Measure*, *Matthew Correlation Coefficient (MCC)* and *Area under the ROC*  
232 *curve (AUC)* as our evaluation metrics.

233 When comparing the performance of the computerized methods and our  
234 proposed techniques, CNNs performed better in the binary classification  
235 of ischaemia than infection despite more imbalanced data in the ischaemia  
236 dataset, due to more cases of non-ischaemia in the dataset. The average per-  
237 formance of all the models in terms of accuracy in the ischaemia dataset was  
238 83.3% which is notably better than the average accuracy of 65.8% in infection  
239 dataset. Similarly, *MCC Score* and *AUC Score* are considered to be viable  
240 performance measures to compare the classification results. We obtained an  
241 average *MCC Score* and *AUC Score* for ischaemia classification of 67.1% and



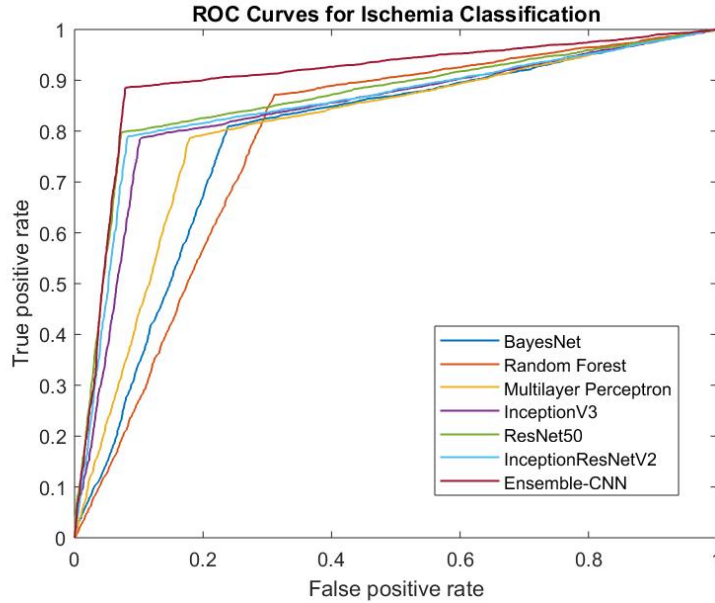


Figure 8: ROC curve for all TML and CNN methods for ischaemia classification.

242 83.2% respectively, as compared to the infection classification of 32.3% and  
 243 65.8% respectively. The ROC curves for all the algorithms, including TML  
 244 and CNNs for binary classification of ischaemia and infection, are shown in  
 245 Fig. 8 and 9. When comparing the performances in ischaemia classification  
 246 of TML and CNNs, CNNs (86.5%) performed better than the TML models  
 247 (79%). Similarly, in infection classification, the accuracy of CNNs (68.4%)  
 248 performed better than TML (62.1%) with a margin of 6.3%. Notably, En-  
 249 semble CNN method achieved the highest score in all performance measures  
 250 in both ischaemia and infection classification.

251 *Sensitivity* and *Specificity* are considered important performance mea-  
 252 sures in medical imaging. The ensemble method yielded high *Sensitivity* for  
 253 the ischaemia dataset with a margin of 6.9% from the second best perform-  
 254 ing algorithm multilayer perceptron. Interestingly, a multilayer perceptron  
 255 performed worst in the *Specificity* with a score of 79.5%. For *Specificity* in  
 256 the ischaemia dataset, the ensemble method again obtained the highest score  
 257 of 92.9% which is marginally better than ResNet50 (92.7%).

258 In infection classification, both TML and CNN methods received mod-  
 259 erate scores in the performance measures. Again, CNN methods performed

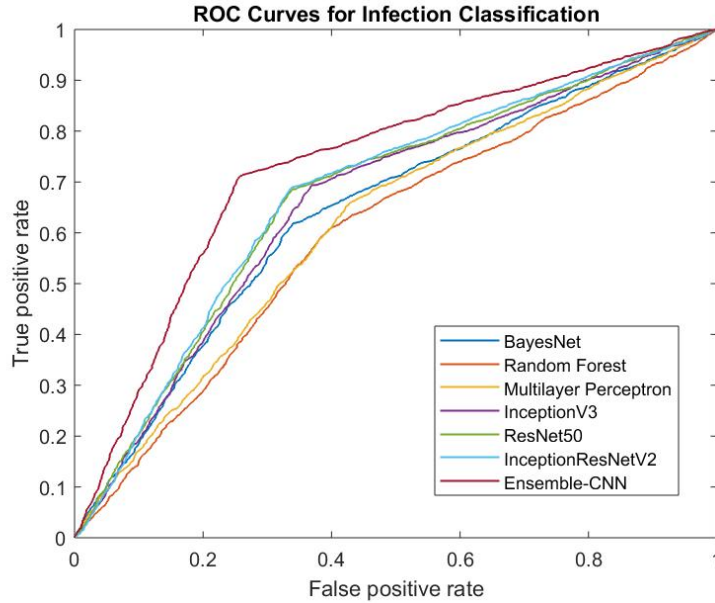


Figure 9: ROC curve for all TML and CNN methods for Infection classification.

260 better than TML methods achieving the highest score in all performance  
 261 measures. The Ensemble CNN method performed better than other CNN  
 262 classifiers especially for *Specificity* with a score of 74.4% in infection classi-  
 263 fication with a notable margin of 8% than the second-best performing algo-  
 264 rithm InceptionResNetV2(66.4%). For *Sensitivity*, all the CNNs performed  
 265 marginally well with Ensemble method achieving the highest score of 70.9%.  
 266 When comparing the performance of TML methods, Multilayer Perceptron  
 267 (68.0%) performed well in *Sensitivity*, whereas BayesNet (66%) better in  
 268 *Specificity*.

#### 269 4.1. Experimental Analysis and Discussion

270 Assessment of DFU with computerized methods is very important for  
 271 supporting global healthcare systems through improving triage and monitor-  
 272 ing procedures and reducing hospital time for patients and clinicians. This  
 273 preliminary experiment is focused on automatically identifying the important  
 274 conditions of ischaemia and infection of DFU. The main aim of this exper-  
 275 iment was to identify ischaemia and infection from images of the feet using  
 276 machine learning. We have illustrated examples of correctly and incorrectly  
 277 classified cases in both binary classifications of ischaemia (Fig. 10 and 11)

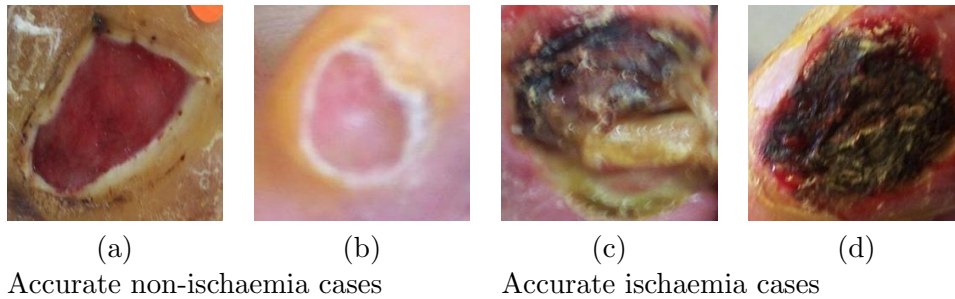


Figure 10: Examples of correctly classified cases by Ensemble-CNN on ischaemia dataset. (a) and (b) represent non-ischaemia cases. (c) and (d) represent ischaemia cases.

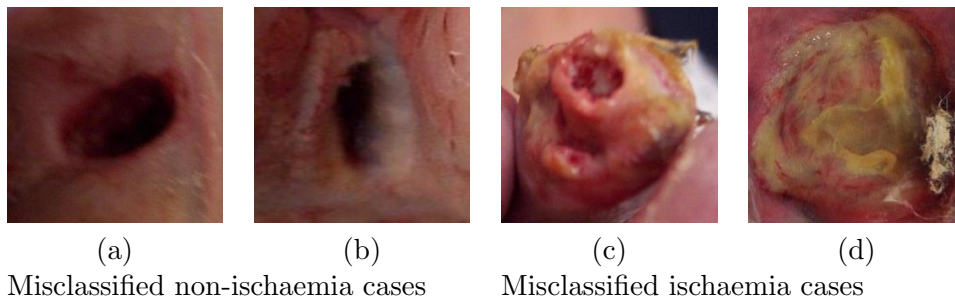


Figure 11: Examples of misclassified cases by Ensemble-CNN on ischaemia dataset. (a) and (b) represents non-ischaemia cases. (c) and (d) represents ischaemia cases.

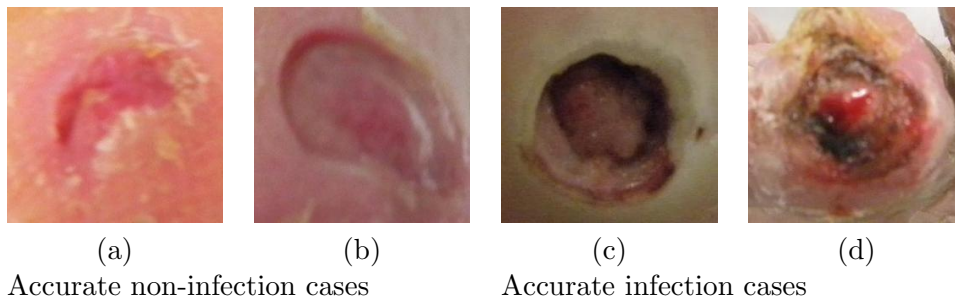


Figure 12: Examples of correctly classified cases by Ensemble-CNN on Infection dataset. (a) and (b) represents non-infection cases. (c) and (d) represents infection cases.

278 and infection (Fig. 12 and 13). As for the misclassified cases, there are huge  
 279 intra-class dissimilarities and inter-class similarities between (1) infection and  
 280 non-infection; (2) ischaemia and non-ischaemia cases in the DFU that make  
 281 classifiers difficult to predict the correct class. Additionally, there are other

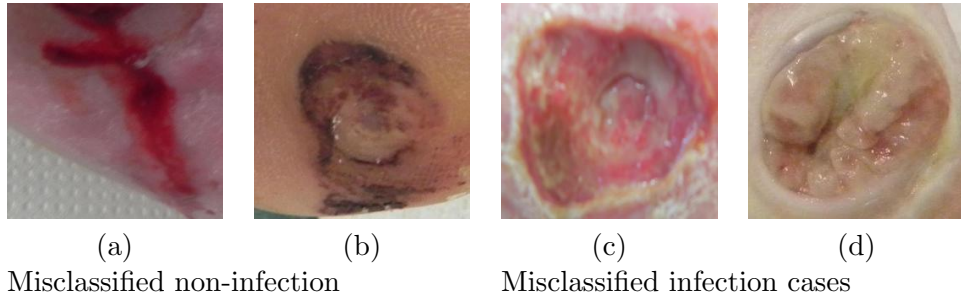


Figure 13: Examples of misclassified cases by Ensemble-CNN on Infection dataset. (a) and (b) represents non-infection cases. (c) and (d) represents infection cases.

282 influencing factors in the classification of these conditions such as lighting  
 283 conditions, marks and skin tone. In misclassified cases of non-ischaemia as  
 284 shown in Fig. 11, the cases (a) and (b) are hindered by the lighting condi-  
 285 tion (shadow) respectively, whereas in the (c) and (d) misclassified ischaemia  
 286 cases, the ischaemia features may be too subtle to be recognised from the  
 287 images by the algorithm. Alternatively it is likely we needed a more sensitive  
 288 objective measure of the ground truth from vascular assessments. We found  
 289 that shadows are particularly problematic because machine learning algo-  
 290 rithms can be deceived by shadows especially in determining the important  
 291 conditions such as ischaemia. In Fig. 13, misclassified cases of non-infection,  
 292 the presence of blood in the case (a), whilst case (b) belongs to one of the  
 293 rare cases with the presence of ischaemia and non-infection. In misclassi-  
 294 fied infection cases, the visual indicators of infection were likely too subtle,  
 295 or we needed more sensitive objective ground truth provided through blood  
 296 analysis.

297 In this work, we used the proposed natural data-augmentation with the  
 298 help of DFU localisation to create DFU patches from full-size foot images.  
 299 These patches are useful to focus more on finding the visual indicators for  
 300 important factors of DFU such as infection and ischaemia. Then, we inves-  
 301 tigated the use of both TML and CNNs to determine these conditions as  
 302 binary classification. In this experiment, we received very good performance  
 303 in terms of correctly classifying ischaemia despite the imbalanced cases in  
 304 the DFU dataset. However, in the case of infection, the classifiers did not  
 305 perform as well, since the condition of infection is hard to recognise from  
 306 the foot images even by experienced medical experts specialized in DFU and  
 307 therefore likely requires ground truth determined using objective blood tests

308 to identify bacterial infection.

309 Current research focuses on ischaemia and infection recognition in med-  
310 ical classification systems, which requiring the guidance of medical experts  
311 specialized in DFU. To develop a computer-aided tool for medical experts in  
312 remote foot analysis, i.e. a remote DFU diagnosis system, the following are  
313 challenges need to be addressed:

- 314 1. Recognition of the ischaemia and infection with machine learning al-  
315 gorithms as an important proof-of-concept study for foot pathologies  
316 classification. Further analysis of each pathology on foot images is  
317 required according to the medical classification systems, such as the  
318 University of Texas Classification of DFU [8] and SINBAD Classifica-  
319 tion System [9]. This requires close collaboration with medical experts  
320 specialized in DFU.
- 321 2. Deep learning algorithms need substantial datasets to obtain very good  
322 accuracy, especially for medical imaging. This experiment included an  
323 imbalanced DFU dataset (1459 foot images) for both ischaemia and in-  
324 fection conditions. In the future, if these algorithms were to train with  
325 a larger number of a more balanced dataset, it can possibly improve  
326 the recognition of ischaemia and infection.
- 327 3. A study of the performance of algorithms on different types of cap-  
328 turing devices is an important aspect of future work. This experi-  
329 ment evaluates the performance of machine learning algorithms on the  
330 DFU dataset collected with different cameras (heterogeneous sources of  
331 data). This leads to more variability of image characteristics. Since the  
332 algorithms have to deal with more heterogeneous patterns and charac-  
333 teristics that are not intrinsic to the pathology itself. In this experi-  
334 ment, we know that three types of devices were used, we do not have  
335 the information on the association of images and the type of devices.
- 336 4. The current ground truth is based on visual inspection by experts only  
337 and not supported by the medical notes or clinical tests (vascular as-  
338 sessment for ischaemia and blood tests to identify the presence of any  
339 bacterial infection). Furthermore, DFU images were debrided before  
340 these images were captured. Hence, the debridement of DFU removes  
341 important visual indicators of infection such as colored exudate. There-  
342 fore, the sensitivity and specificity of these algorithms could be further  
343 improved in the future, by feeding in ground truth from clinical tests  
344 such as vascular assessments (ischaemia) and blood tests (to identify

- 345 the presence of any bacterial infection).
- 346 5. Current clinical practice obtains the foot photo using different camera  
347 models, poses and illumination. It is a great challenge for a computer  
348 algorithm to predict the depth and the size of the wound based on non-  
349 standardized images. Standardized dataset, such as the data collection  
350 method proposed by Yap et al. [30] will help to increase the accuracy  
351 of the DFU diagnosis system.
- 352 6. Dataset annotation is a laborious process, particularly for medical ex-  
353 perts to label the foot pathologies into 16 classes according to the Uni-  
354 versity of Texas classification system. To reduce the burden upon medi-  
355 cal experts in the delineation and annotation of the dataset, there is  
356 an urgent need to focus on developing unsupervised or self-supervised  
357 machine learning techniques.
- 358 7. Collecting the time-line dataset is crucial for early detection of key  
359 pathologies. This will enable monitoring of foot health and changes lon-  
360 gitudinally, where medical experts and computer algorithms can learn  
361 the early signs of DFU. In the longer-term, the DFU diagnosis system  
362 will be able to predict the healing process of ulcers and prevent DFU  
363 before it happens.
- 364 8. A smart-phone app could be developed for remote triage and moni-  
365 toring of DFU. To scale-up the DFU diagnosis system, the application  
366 should run on multiple devices, irrespective of the platform and/or the  
367 operating system.

## 368 5. Conclusion

369 In this work, we trained various classifiers based on traditional machine  
370 learning algorithms and CNNs to discriminate the conditions of: (1) is-  
371 chaemia and non-ischaemia; and (2) infection and non-infection related to  
372 a given DFU. We found high-performance measures in the binary classifi-  
373 cation of ischaemia, compared to moderate performance by classifiers in the  
374 classification of infection. It is vital to understand the features of both condi-  
375 tions in relation to the DFU (ischaemia and infection) from a computer vision  
376 perspective. Determining these conditions especially infection from the non-  
377 standard foot images is very challenging due to: (1) high visual intra-class  
378 dissimilarities and inter-class similarities between classes; (2) the visual in-  
379 dicators of infection and ischaemia potentially being too subtle in DFU; (3)  
380 objective medical tests for vascular supply and bacterial infection are needed

381 to provide more objective ground truth and further improve the classification  
382 of these conditions; and (4) other factors such as lighting conditions, marks  
383 and skin tone are important to incorporate into the prediction.

384 With a more balanced dataset and improved data capturing of DFU,  
385 the performance of these methods could be improved in the future. Further  
386 optimization in hyper-parameters of both deep learning and traditional ma-  
387 chine learning methods could improve the performance of algorithms on this  
388 dataset. Ground truths enhanced by clinical tests for the ischaemia and infec-  
389 tion may provide further insight and further improvement of algorithms even  
390 where there is no apparent visual indicator by eye. In the case of infection  
391 even after debridement, ground truth informed by blood tests for infection  
392 may yield improvements to sensitivity and specificity even in the absence of  
393 overtly obvious visual indicators. This work has the potential for technology  
394 that may transform the recognition and treatment of diabetic foot ulcers and  
395 lead to a paradigm shift in the clinical care of the diabetic foot.

## 396 **Acknowledgements**

397 The authors express their gratitude to Lancashire Teaching Hospitals  
398 and the clinical experts for their extensive support and contribution in car-  
399 rying out this research. We would like to thank Kim's English Corner  
400 (<https://kimsenglishcorner.com>) for proofreading.

## 401 **Reference**

- 402 [1] J. D. Santilli, S. M. Santilli, Chronic critical limb ischemia: diagnosis,  
403 treatment and prognosis., *American family physician* 59 (7) (1999) 1899–  
404 1908.
- 405 [2] M. Albers, A. C. Fratezi, N. De Luccia, Assessment of quality of life of  
406 patients with severe ischemia as a result of infrainguinal arterial occlu-  
407 sive disease, *Journal of vascular surgery* 16 (1) (1992) 54–59.
- 408 [3] L. Prompers, M. Huijberts, J. Apelqvist, E. Jude, A. Piaggese,  
409 K. Bakker, et al., High prevalence of ischaemia, infection and serious  
410 comorbidity in patients with diabetic foot disease in europe. baseline  
411 results from the eurodiale study, *Diabetologia* 50 (1) (2007) 18–25.

- 412 [4] B. A. Lipsky, A. R. Berendt, P. B. Cornia, J. C. Pile, E. J. Peters,  
413 D. G. Armstrong, et al., 2012 infectious diseases society of america clin-  
414 ical practice guideline for the diagnosis and treatment of diabetic foot  
415 infections, *Clinical infectious diseases* 54 (12) (2012) e132–e173.
- 416 [5] L. A. Lavery, D. G. Armstrong, R. P. Wunderlich, J. Tredwell, A. J.  
417 Boulton, Diabetic foot syndrome: evaluating the prevalence and inci-  
418 dence of foot pathology in mexican americans and non-hispanic whites  
419 from a diabetes disease management cohort, *Diabetes care* 26 (5) (2003)  
420 1435–1438.
- 421 [6] G. H. Skrepnek, J. L. Mills, L. A. Lavery, D. G. Armstrong, Health care  
422 service and outcomes among an estimated 6.7 million ambulatory care  
423 diabetic foot cases in the us, *Diabetes Care* 40 (7) (2017) 936–942.
- 424 [7] F. W. Wagner, The diabetic foot, *Orthopedics* 10 (1) (1987) 163–172.
- 425 [8] L. A. Lavery, D. G. Armstrong, L. B. Harkless, Classification of diabetic  
426 foot wounds, *The Journal of Foot and Ankle Surgery* 35 (6) (1996) 528–  
427 531.
- 428 [9] P. Ince, Z. G. Abbas, J. K. Lutale, A. Basit, S. M. Ali, F. Chohan,  
429 S. Morbach, et al., Use of the sinbad classification system and score  
430 in comparing outcome of foot ulcer management on three continents,  
431 *Diabetes care* 31 (5) (2008) 964–967.
- 432 [10] J. J. van Netten, D. Clark, P. A. Lazzarini, M. Janda, L. F. Reed, The  
433 validity and reliability of remote diabetic foot ulcer assessment using  
434 mobile phone images, *Scientific Reports* 7 (1) (2017) 9480.
- 435 [11] V. Gulshan, L. Peng, M. Coram, M. C. Stumpe, D. Wu,  
436 A. Narayanaswamy, et al., Development and validation of a deep learn-  
437 ing algorithm for detection of diabetic retinopathy in retinal fundus  
438 photographs, *Jama* 316 (22) (2016) 2402–2410.
- 439 [12] A. Esteva, B. Kuprel, R. A. Novoa, J. Ko, S. M. Swetter, H. M. Blau,  
440 et al., Dermatologist-level classification of skin cancer with deep neural  
441 networks, *Nature* 542 (7639) (2017) 115–118.



- 442 [13] A. Krizhevsky, I. Sutskever, G. E. Hinton, Imagenet classification with  
443 deep convolutional neural networks, in: *Advances in neural information*  
444 *processing systems*, 2012, pp. 1097–1105.
- 445 [14] F. Veredas, H. Mesa, L. Morente, Binary tissue classification on wound  
446 images with neural networks and bayesian classifiers, *IEEE transactions*  
447 *on medical imaging* 29 (2) (2009) 410–427.
- 448 [15] H. Wannous, Y. Lucas, S. Treuillet, Enhanced assessment of the wound-  
449 healing process by accurate multiview tissue classification, *IEEE trans-*  
450 *actions on Medical Imaging* 30 (2) (2010) 315–326.
- 451 [16] L. Wang, P. Pedersen, E. Agu, D. Strong, B. Tulu, Area determina-  
452 tion of diabetic foot ulcer images using a cascaded two-stage svm based  
453 classification, *IEEE Transactions on Biomedical Engineering* (2016).
- 454 [17] M. H. Yap, M. Goyal, F. M. Osman, R. Martí, E. Denton, A. Juette,  
455 et al., Breast ultrasound lesions recognition: end-to-end deep learning  
456 approaches, *Journal of Medical Imaging* 6 (1) (2018) 011007.
- 457 [18] E. Ahmad, M. Goyal, J. S. McPhee, H. Degens, M. H. Yap, Semantic  
458 segmentation of human thigh quadriceps muscle in magnetic resonance  
459 images, arXiv preprint arXiv:1801.00415 (2018).
- 460 [19] M. Goyal, N. D. Reeves, A. K. Davison, S. Rajbhandari, J. Spragg,  
461 M. H. Yap, Dfunet: convolutional neural networks for diabetic foot ulcer  
462 classification, *IEEE Transactions on Emerging Topics in Computational*  
463 *Intelligence* (2018) 1–12doi:10.1109/TETCI.2018.2866254.
- 464 [20] M. Goyal, M. H. Yap, N. D. Reeves, S. Rajbhandari, J. Spragg, Fully  
465 convolutional networks for diabetic foot ulcer segmentation, in: *2017*  
466 *IEEE International Conference on Systems, Man, and Cybernetics*  
467 *(SMC)*, 2017, pp. 618–623. doi:10.1109/SMC.2017.8122675.
- 468 [21] M. Goyal, N. D. Reeves, S. Rajbhandari, M. H. Yap, Robust methods for  
469 real-time diabetic foot ulcer detection and localization on mobile devices,  
470 *IEEE Journal of Biomedical and Health Informatics* 23 (4) (2019) 1730–  
471 1741. doi:10.1109/JBHI.2018.2868656.
- 472 [22] C. Wang, X. Yan, M. Smith, K. Kochhar, M. Rubin, S. M. Warren, et al.,  
473 A unified framework for automatic wound segmentation and analysis

- 474 with deep convolutional neural networks, in: Engineering in Medicine  
475 and Biology Society (EMBC), 2015 37th Annual International Confer-  
476 ence of the IEEE, IEEE, 2015, pp. 2415–2418.
- 477 [23] J. L. Mills Sr, M. S. Conte, D. G. Armstrong, F. B. Pomposelli,  
478 A. Schanzer, A. N. Sidawy, et al., The society for vascular surgery lower  
479 extremity threatened limb classification system: risk stratification based  
480 on wound, ischemia, and foot infection (wif), *Journal of vascular surgery*  
481 59 (1) (2014) 220–234.
- 482 [24] M. Goyal, M. H. Yap, Region of interest detection in dermoscopic images  
483 for natural data-augmentation, arXiv preprint arXiv:1807.10711 (2018).
- 484 [25] J. Huang, V. Rathod, C. Sun, M. Zhu, A. Korattikara, A. Fathi, et al.,  
485 Speed/accuracy trade-offs for modern convolutional object detectors,  
486 arXiv preprint arXiv:1611.10012 (2016).
- 487 [26] R. Achanta, A. Shaji, K. Smith, A. Lucchi, P. Fua, S. Süsstrunk, Slic  
488 superpixels, Tech. rep. (2010).
- 489 [27] C. Szegedy, V. Vanhoucke, S. Ioffe, J. Shlens, Z. Wojna, Rethinking  
490 the inception architecture for computer vision, in: Proceedings of the  
491 IEEE Conference on Computer Vision and Pattern Recognition, 2016,  
492 pp. 2818–2826.
- 493 [28] C. Szegedy, S. Ioffe, V. Vanhoucke, Inception-v4, inception-resnet and  
494 the impact of residual connections on learning, CoRR abs/1602.07261  
495 (2016). arXiv:1602.07261.  
496 URL <http://arxiv.org/abs/1602.07261>
- 497 [29] K. He, X. Zhang, S. Ren, J. Sun, Deep residual learning for image  
498 recognition, in: Proceedings of the IEEE conference on computer vision  
499 and pattern recognition, 2016, pp. 770–778.
- 500 [30] M. H. Yap, K. E. Chatwin, C.-C. Ng, C. A. Abbott, F. L. Bowling,  
501 S. Rajbhandari, et al., A new mobile application for standardizing di-  
502 abetic foot images, *Journal of diabetes science and technology* 12 (1)  
503 (2018) 169–173.